Clinical Cancer Research

Long Noncoding RNA *SChLAP1* Forms a Growth-Promoting Complex with HNRNPL in Human Glioblastoma through Stabilization of ACTN4 and Activation of NF-κB Signaling

Jianxiong Ji[1], Ran Xu[1], Kaikai Ding[1], Guoqing Bao[2], Xin Zhang[1], Bin Huang[1], Xinyu Wang[1], Aurora Martinez[3], Xiuying Wang[2], Gang Li[1], Hrvoje Miletic[3,4,5], Frits Thorsen[3,4,6], Rolf Bjerkvig[3,4,7], Lei Xiang[8], Bo Han[8], Anjing Chen[1,9], Xingang Li[1], and Jian Wang[1,3,4]

Abstract

Purpose: Long noncoding RNAs (lncRNA) have essential roles in diverse cellular processes, both in normal and diseased cell types, and thus have emerged as potential therapeutic targets. A specific member of this family, the SWI/SNF complex antagonist associated with prostate cancer 1 (*SChLAP1*), has been shown to promote aggressive prostate cancer growth by antagonizing the SWI/SNF complex and therefore serves as a biomarker for poor prognosis. Here, we investigated whether *SChLAP1* plays a potential role in the development of human glioblastoma (GBM).

Experimental Design: RNA-ISH and IHC were performed on a tissue microarray to assess expression of *SChLAP1* and associated proteins in human gliomas. Proteins complexed with *SChLAP1* were identified using RNA pull-down and mass spectrometry. Lentiviral constructs were used for functional analysis *in vitro* and *in vivo*.

Results: *SChLAP1* was increased in primary GBM samples and cell lines, and knockdown of the lncRNA suppressed growth. *SChLAP1* was found to bind heterogeneous nuclear ribonucleoprotein L (HNRNPL), which stabilized the lncRNA and led to an enhanced interaction with the protein actinin alpha 4 (ACTN4). *ACTN4* was also highly expressed in primary GBM samples and was associated with poorer overall survival in glioma patients. The *SChLAP1*–HNRNPL complex led to stabilization of ACTN4 through suppression of proteasomal degradation, which resulted in increased nuclear localization of the p65 subunit of NF-κB and activation of NF-κB signaling, a pathway associated with cancer development.

Conclusions: Our results implicated *SChLAP1* as a driver of GBM growth as well as a potential therapeutic target in treatment of the disease.

Introduction

Glioblastoma multiforme (GBM) accounts for nearly half of all primary brain tumors in adults (1). Aggressive growth is a hallmark of GBM, which exhibits a median survival time of only 14 to 16 months following standard-of-care therapy (2, 3), and poses a considerable challenge in GBM treatment (4). Rigorous molecular analysis has revealed many factors, such as EGF, IGF, TGFβ, and downstream effectors involved in the uncontrolled growth of GBM (5). Despite this knowledge, current treatment of GBM has limited efficacy, thus rendering the field desperate for novel therapeutic approaches.

Although somatic mutations clearly contribute to change in expression of many of these factors, a variety of other mechanisms, including dysregulation of noncoding RNAs, are recognized as having significant roles in the disease. One class of these RNAs, the long noncoding RNAs (lncRNA), have been shown to regulate gene expression, as signals, decoys, guides, and scaffolds (6). LncRNAs play critical roles in many biological processes taking place in human cancers, including gliomas, such as proliferation, apoptosis, angiogenesis, stemness, drug resistance, migration, and invasion (7). In the case of GBM, lncRNAs *NEAT1* and *TP73-AS1* promote cell growth through different mechanisms, mediating chromatin modification (8) and acting as a sponge for *mir-142*, respectively (9).

[1]Department of Neurosurgery, Qilu Hospital of Shandong University and Brain Science Research Institute, Shandong University, Key Laboratory of Brain Functional Remodeling, Shandong, 107# Wenhua Xi Road, Jinan, China. [2]Biomedical and Multimedia Information Technologies Group, School of Information Technologies, The University of Sydney, J12/1 Cleveland St, Darlington, Sydney, New South Wales, Australia. [3]Department of Biomedicine, University of Bergen, Bergen, Norway. [4]K. G. Jebsen Brain Tumor Research Center, Department of Biomedicine, University of Bergen, Bergen, Norway. [5]Department of Pathology, Haukeland University Hospital, Bergen, Norway. [6]The Molecular Imaging Center, Department of Biomedicine, University of Bergen, Bergen, Norway. [7]Department of Oncology, Luxembourg Institute of Health, Luxembourg. [8]Department of Pathology, Qilu Hospital of Shandong University, Jinan, China. [9]School of Medicine, Shandong University, Jinan, China.

Note: Supplementary data for this article are available at Clinical Cancer Research Online (http://clincancerres.aacrjournals.org/).

J. Ji and R. Xu contributed equally to this article.

Corresponding Authors: Jian Wang, University of Bergen, Jonas Lies vei 91, Bergen 5009, Norway. Phone: 8605-31821-66615; Fax: 8605-31821-66615; E-mail: Jian.Wang@uib.no; Anjing Chen, chenaj@sdu.edu.cn; and Xingang Li, lixg@sdu.edu.cn

Clin Cancer Res 2019;25:6868–81

doi: 10.1158/1078-0432.CCR-19-0747

Translational Relevance

LncRNAs have emerged as critical drivers in diverse cancers, and thus represent a novel druggable molecular target. We show that *SChLAP1*, an lncRNA, promoted the growth of GBM cells *in vitro* and *in vivo*. In pull-down assays, we identified HNRNPL as an associated protein, and knockdown of HNRNPL abrogated the oncogenic effects of *SChLAP1* on GBM growth. This complex facilitated the association of HNRNPL with ACTN4, a mediator in NF-κB signaling, and inhibited proteasome-mediated degradation of this protein. The resultant stabilization of ACTN4 led to activation of downstream NF-κB signaling. Overall, our results identify *SChLAP1* as a potential oncogene in the development of GBM through HNRNPL-mediated ACTN4 stabilization and may provide a potential molecular target to be exploited in the therapeutic treatment of GBM.

Another lncRNA well known for its oncogenic role specifically in prostate cancer, is the SWI/SNF complex antagonist associated with prostate cancer 1 (*SChLAP1*). The lncRNA antagonizes the SWI/SNF complex (10), which has been widely recognized as a suppressor in diverse cancers (11). However, the suppressive role of the SWI/SNF complex has been challenged in recent studies showing that the complex can also function as an oncogenic factor in certain cellular contexts (10). For instance, SS18, a subunit of the SWI/SNF complex, acts as a growth promoter in synovial sarcomas through the SS18-SSX fusion protein (12). In addition, we previously demonstrated that *ACTL6A* (*BAF53*), a gene encoding a subunit of the SWI/SNF complex, facilitates the development of human glioma (10, 13).

In this study, we investigated the role of *SChLAP1* in glioma progression. Elevated expression of *SChLAP1* was associated with increasing tumor grade in human gliomas. We used coimmunoprecipitation (co-IP) assays coupled with mass spectrometry to identify protein binding partners of *SChLAP1*. This approach revealed an RNA-binding protein, heterogeneous nuclear ribonucleoprotein L (HNRNPL), in complex with *SChLAP1*. We demonstrate that this complex leads to protein stabilization of ACTN4 and ultimately activation of NF-κB signaling pathway. A specific RNA recognition motif (RRM) within HNRNPL binds to exon 2 of *SChLAP1*, thus providing a binding interface that may serve as a promising drug target in the treatment of GBM.

Materials and Methods

Ethics statement

All primary glioma tissue samples ($n = 112$) were obtained from the Department of Neurosurgery at Qilu Hospital of Shandong University (Jinan, China) from individuals consenting to the use of their tissues for research purposes. Clinicopathologic characteristics are provided in Supplementary Table S1. Nonneoplastic brain tissue samples (NBT; $n = 10$) were obtained from the Department of Pathology at Qilu Hospital of Shandong University. Research strategies pertaining to human tissues and animals were all approved and performed according to the regulations outlined by the Research Ethics Committee of Shandong University and the Ethics Committee of Qilu Hospital, in accordance with the Declaration of Helsinki (for humans) and the U.S. Public Health Service Policy on Human Care and Use of Laboratory Animals (2015 reprint; for mice).

Cell culture, transient transfection, and lentivirus infection

Human glioblastoma cell lines (U118MG and LN229) and the human embryonic kidney cell line 293 (HEK293) were purchased from the ATCC. All human cell lines were authenticated and submitted for short tandem repeat analysis (Cell Cook Biotech Co. Ltd.). Normal human astrocytes (NHA), primary GBM#P3 cells and BG7 glioma stem cells (GSC) were kindly gifted by Prof. Rolf Bjerkvig (University of Bergen, Bergen, Norway). Cells were maintained in DMEM (Life Technologies/Thermo Fisher Scientific) supplemented with 10% FBS (Thermo Fisher Scientific). GBM#P3 and GSC BG7 cells were cultured in serum-free DMEM/F12 medium (Gibco/Thermo Fisher Scientific) supplemented with 2% B27 Neuro Mix (Thermo Fisher Scientific), EGF (20 ng/mL; Thermo Fisher Scientific), and basic FGF (10 ng/mL; Thermo Fisher Scientific).

Transient transfections for siRNAs and plasmids were performed with Lipofectamine 2000 or 3000 (Thermo Fisher Scientific). The sequences of siRNAs used are listed in Supplementary Table S2, and plasmids used are listed in Supplementary Table S3.

Lentiviral constructs were used for stable knockdown of *SChLAP1* in LN229 and GBM#P3 cells and HNRNPL in U118MG- and BG7-*SChLAP1*-OE cells with short hairpin RNAs (shRNA; OBiO Technology) and for stable ectopic expression of *SChLAP1* in U118MG and BG7 cells. In addition to the construct expressing full-length *SChLAP1*, an exon 2 deletion mutant of *SChLAP1* (*SChLAP1*-Δexon 2) and *SChLAP1* antisense (*SChLAP1*-AS; OBiO Technology) constructs were also used to infect cells. After 48 hours, infected cells were cultured in media containing puromycin (2 μg/mL; Thermo Fisher Scientific) for 2 weeks to select for stable expression. The sequences of shRNAs used are listed in Supplementary Table S2.

Subcellular fractionation

Nuclear and cytoplasmic cellular subfractions of LN229 and U118MG cells were prepared using Nuclear and Cytoplasmic Extraction Reagents (Thermo Fisher Scientific) according to the manufacturer's instructions. Subcellular distribution of proteins, including p65, were determined using Western blot analysis. GAPDH and histone H3 served as loading controls for cytosolic and nuclear protein fractions, respectively.

RNA *in situ* hybridization and evaluation of *SChLAP1* staining

RNA *in situ* hybridization (RNA-ISH) was performed according to the manufacturer's instructions (Boster Bio-Technology Company). Briefly, paraffin-embedded samples were deparaffinized with xylene and rehydrated with diluted reagent grade ethanol. Human glioma tissue microarrays were digested with proteinase K for 15 minutes, hybridized at 37°C overnight with a 5′-digoxin-labeled probe targeting *SChLAP1* (5′-ACACT CACTG CGAGG GTCCG CGGCT TCATT CTTGA AGTGA-3′), and incubated with HRP-conjugated anti-digoxin antibody for 30 minutes at room temperature. Diaminobenzidine was used as the HRP substrate in the color reaction for staining.

The RNA-ISH–stained samples were reviewed and evaluated by two pathologists in a blinded study using scoring methods detailed in Supplementary Materials and Methods.

RNA-FISH

RNA-FISH was performed according to the manufacturer's instructions (Boster Bio-Technology Company). Cells were seeded on coverslips, fixed with 4% paraformaldehyde, and incubated with a 3′-digoxin-labeled *SChLAP1* probe. For fluorescence detection, cells were incubated with biotin-mouse anti-digoxin antibody and subsequently streptavidin-conjugated Cy3. Nuclei were counterstained with DAPI. Images were acquired under confocal microscopy (LSM780, Zeiss).

qRT-PCR

Nuclear and cytoplasmic RNA was isolated using the PARIS Kit (Thermo Fisher Scientific). Total RNA was isolated from cells using TRIzol Reagent (Thermo Fisher Scientific). RNA (2 μg) was reverse transcribed into cDNA using the High Efficient Reverse Transcription Kit (Toyobo Life Science) according to the manufacturer's protocol. Quantitative PCR was performed using SYBR premix Ex Taq (Takara) on the Real-Time PCR Detection System (480II, Roche). GAPDH served as the internal control for normalization. Primers used for PCR are listed in Supplementary Table S4.

IHC, immunofluorescence, and immunoblotting

IHC, immunofluorescence, and immunoblotting were performed as described previously (13). All antibodies used and the scoring system for ACTN4 IHC staining used are described in detail in Supplementary Materials and Methods.

Co-IP and mass spectrometry analysis

Cells were lysed in IP lysis buffer (Pierce) containing a protease inhibitor cocktail (Sigma-Aldrich). Total lysates (200 μg; 1 μg/μL) were incubated with primary antibodies (4 μL) or IgG (4 μL) overnight at 4°C with gentle shaking followed by Protein A/G magnetic beads (Thermo Fisher Scientific) for 2 hours at room temperature. The immunoprecipitated complexes were immunoblotted or subjected to mass spectrometry analysis (ekspertTM-nanoLC; AB Sciex TripleTOF 5600-plus; SCIEX). Results of LC-MS/MSF were analyzed using Proteinpilot software. For the ubiquitination assay, cells were treated with 20 μmol/L MG132 for 6 hours before lysis, followed by co-IP and Western blot analysis. The antibodies used are described in Supplementary Materials and Methods.

Biotin-labeled RNA pull-down and mass spectrometry analysis

Human *SChLAP1* cDNAs (sense and antisense; OBiO Technology) and truncated constructs were transcribed *in vitro* using the TranscriptAid T7 High Yield Transcription Kit (Thermo Fisher Scientific). Resultant transcripts were 3′ end labeled with biotin using the RNA 3′ End Desthiobiotinylation Kit (Thermo Fisher Scientific) to generate RNA probes for RNA pull-downs, which were performed using the Magnetic RNA-Protein Pull-Down Kit (Thermo Fisher Scientific), according to the manufacturer's instructions. Eluted proteins were detected by Western blot or mass spectrometry analysis.

Cross-link RNA immunoprecipitation

RNA immunoprecipitation (RIP) assays were performed using the EZ-Magna RIP RNA-Binding Protein Immunoprecipitation Kit (Merck Millipore). Briefly, cells were cross-linked with 1% formaldehyde and collected in lysis buffer containing a protease inhibitor cocktail (Sigma) and an RNase inhibitor. Magnetic beads were preincubated with an anti-rabbit IgG or antibody specific for HNRNPL (Abcam, ab6106) for 30 minutes at room temperature, followed by incubation with lysates at 4°C overnight. Coprecipitated RNAs were eluted and purified, and then detected by RT-PCR with specific primers (Supplementary Table S4). Total RNA (input) served as the internal control.

Cycloheximide chase

LN229 and GBM#P3 cells were infected with lentivirus containing shRNA targeting *SChLAP1* (OBiO Technology). U118MG and BG7 cells were infected with lentivirus for ectopic expression of full-length *SChLAP1* (OBiO Technology). After 48 hours, cycloheximide (25 μg/mL; Apexbio) was added to the culture medium to inhibit translation, and cell lysates were prepared at 0, 4, 8, or 12 hours. Protein (20 μg) was examined using Western blot analysis.

Colony-forming assay

After infection, cells (1.0×10^3/well) were seeded into 6-well plates and cultured for an additional 2 weeks. Cells were then fixed with 4% paraformaldehyde (Solarbio) and stained with 5% crystal violet. Colonies containing more than 50 cells were counted. Experiments were performed in triplicate.

Cell number counting

After infection, cells (1.0×10^5/well) were seeded into 6-well plates. Cells were harvested through trypsinization and counted every 24 hours. Experiments were performed in triplicate.

Luciferase reporter assays

The NF-κB firefly-luciferase (Promega) and *Renilla* reporter constructs (100 ng each) were cotransfected into modified U118MG and LN229 cells using Lipofectamine 3000 (Thermo Fisher Scientific). Luciferase assays were performed 24 hours later using the Dual-Luciferase Reporter Assay Kit (Promega). *Renilla* activity was used to normalize luciferase reporter activity. The promoterless firefly luciferase vector pGL4.15 served as the negative control (NC).

Animal studies

After infection, luciferase-expressing human glioma cell lines (3×10^5 cells suspended in 10 μL PBS) were implanted into the frontal lobes of 4-week-old athymic nude mice (Shanghai SLAC Laboratory Animal Co., Ltd.) using a stereotactic apparatus (KDS310, KD Scientific). Tumor growth was examined at 6, 12, and 24 days after implanation with bioluminescence imaging (IVIS Spectrum in vivo imaging system, PerkinElmer). Animals were sacrificed by cervical dislocation if they showed any symptoms of continuous discomfort, such as severe hunchback posture, decreased motion or activity, apathy, dragging of legs, or more than 20% weight loss.

Database and gene enrichment analysis

Survival analysis using *ACTN4* expression levels was performed using Rembrandt (http://www.betastasis.com/glioma/rembrandt/) and CGGA (http://www.cgga.org.cn/) databases. Enrichment analysis of *ACTN4* was performed using clinical data from patients in the CGGA database. Pearson correlation coefficients >0.4 and P values <0.05 were used to identify genes correlated with *ACTN4*.

Molecular modeling of HNRNPL

Visualization of the molecular models was performed with Discovery Studio Visualiser (Biovia). Molecular surfaces colored for interpolated charge were also developed in Discovery Studio Visualiser. The structural model of HNRNPL was created using i-Tasser (14). The templates used in the structure determination were the NMR structures of the four RRM domains in rat HNRNPL, RRM1 (PDB ID 2MQL/2MQO; without/with RNA), RRM2 (PDB ID 2MQM/2MQP), and RRM3-RRM4 (PDB ID 2MQN/2MQQ), as well as the X-ray structures of RRM3-RRM4 without RNA (PDB ID 3TOH). Rat and human HNRNPL have a sequence identity of 92%.

Statistical analysis

Data are presented as the mean ± the SEM. The Student *t* test for paired data was used to compare mean values. ANOVA was used to analyze potential differences between two groups with continuous variables. Survival curves were estimated using the Kaplan–Meier method and compared using the log-rank test. Correlation between *SChLAP1* and *ACTN4* expression levels was determined using the two-tailed χ^2 test or the Fisher exact test. Statistical analysis was conducted using GraphPad Prism version 7.00 software for Windows (GraphPad). All tests were two-sided, and *P* values <0.05 were considered to be statistically significant.

Results

SChLAP1 is highly expressed in GBM and correlated with poor prognosis in glioma patients

To begin to characterize the role of *SChLAP1* in the development of human glioma, we used RNA-ISH to assess RNA levels of the gene in a cohort of primary tissue samples on a tissue microarray. The histology and distribution of the samples

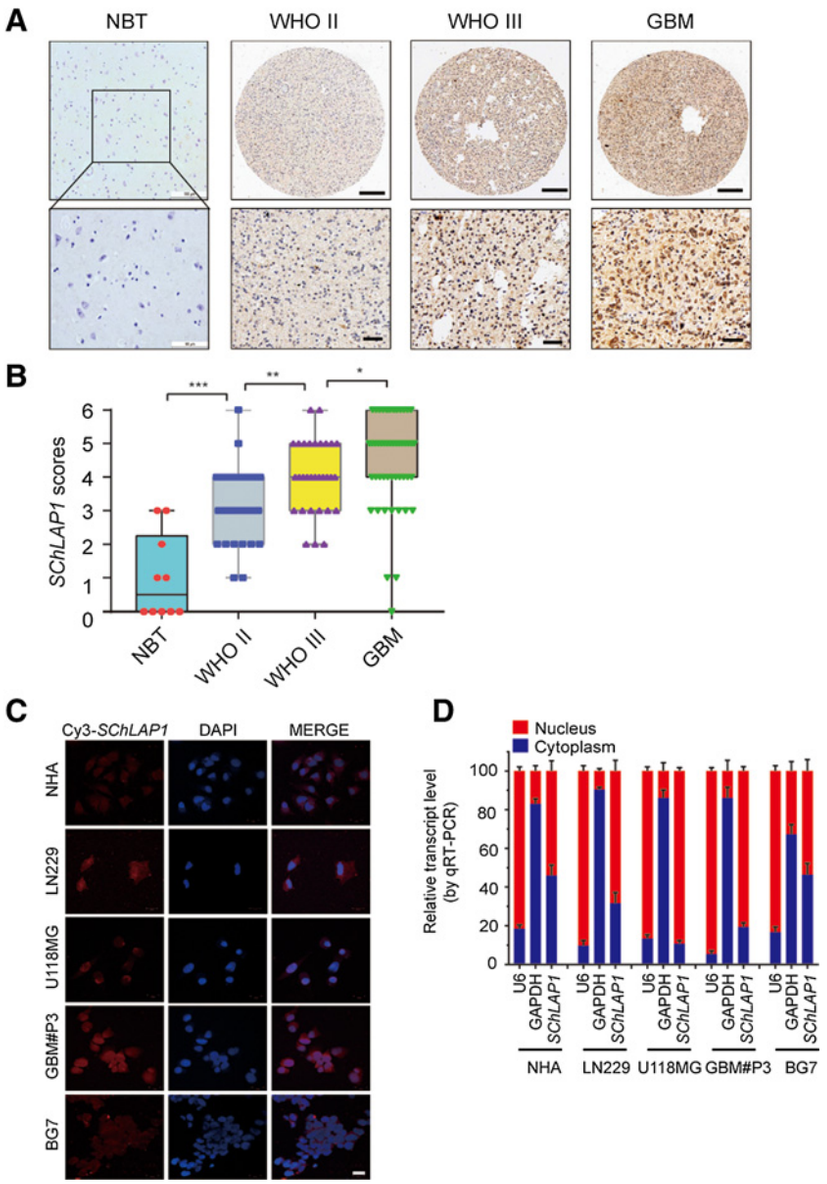

Figure 1.

SChLAP1 is highly expressed in primary GBM samples. **A,** RNA-ISH for *SChLAP1* performed on WHO grade II–IV glioma tissue microarrays and nonneoplastic brain tissues (NBT). Representitave image of NBT was from frontal lobe; scale bar, 100 μm (top) or 50 μm (bottom). For glioma tissue microarrays, scale bar, 200 μm (top) or 50 μm (bottom). **B,** Graphic representation of scoring performed on RNA-ISH staining for *SChLAP1* in primary samples from glioma tissue microarrays and NBT. **C,** RNA-FISH to detect Cy3-*SChLAP1* (red) in NHA, LN229, U118MG, GBM#P3, and BG7 cells. Nuclei were stained with DAPI (blue), and images were merged. Scale bar, 20 μm. **D,** qRT-PCR for *SChLAP1* expression in cytoplasmic and nuclear RNAs isolated from NHA, LN229, U118MG, GBM#P3, and BG7 cells (n.s., not significant; *, $P < 0.05$; **, $P < 0.01$; ***, $P < 0.001$).

was as follows: WHO grade II ($n = 30$), WHO grade III ($n = 31$), WHO grade IV ($n = 51$, GBMs), and nonneoplastic brain (NBT, $n = 10$). *SChLAP1* was preferentially expressed in high-grade glioma ($n = 82$; HGG, WHO grade III–IV) compared with low-grade glioma ($n = 30$; LGG, WHO grade II; Fig. 1A and B; Supplementary Table S5). Expression in nonneoplastic brain tissue samples was nearly absent (Fig. 1A and B; Supplementary Fig. S1A). Increased expression of *SChLAP1* correlated with wild-type *IDH1* ($P = 0.0450$) as well as advanced grade ($P < 0.001$; Supplementary Table S5).

To localize *SChLAP1*, we performed RNA-FISH labeling on NHA, LN229, U118MG, GBM#P3, and BG7 cells *in vitro*. *SChLAP1* was mainly expressed in the nucleus of all four GBM cell lines, with a minor fraction in the cytoplasm (Fig. 1C). However, Cy3-*SChLAP1* was not detected in NHA. These results were consistent with *SChLAP1* localization in human prostate cancer cells (13). We further validated these results by performing qRT-PCR on nuclear and cytoplasmic fractions of RNA obtained from these cell populations. Again, the major portion of *SChLAP1* was in the nucleus (70%–80%), while a lesser fraction (20%–30%) was detected in the cytoplasm in all GBM cell lines tested except in the case of BG7 cells. In these cells, *SChLAP1* mRNA was distributed equally between the nucleus and the cytoplasm (Fig. 1D).

These results demonstrated that *SChLAP1* expression was frequently increased in GBM cells in primary tumor samples and *in vitro*, and mostly localized to the nucleus.

SChLAP1 promotes growth of GBM cells both *in vitro* and *in vivo*

To determine whether the increase in *SChLAP1* promoted or inhibited growth in GBM, we modified *SChLAP1* expression in GBM cells and assessed cell growth *in vitro* and *in vivo*. Gene knockdown studies were performed in LN229 and GBM#P3, which exhibited high levels of *SChLAP1* (Fig. 1C; Supplementary Fig. S5D). In LN229 and GBM#P3 cells transfected with sh-*SChLAP1*-1 and sh-*SChLAP1*-2, *SChLAP1* expression was reduced by approximately 60% (Fig. 2A). Growth curves generated over 72 hours for the different modified cell types versus controls revealed that *SChLAP1* knockdown attenuated proliferation of LN229 and GBM#P3 cells significantly (Fig. 2B). Results from colony formation assays further demonstrated that *SChLAP1* was growth promoting in GBM cells lines LN229 and GBM#P3 *in vitro* (Fig. 2C).

To test growth *in vivo*, modified and control cell lines were orthotopically implanted in mice, and tumor growth was monitored/quantified using bioluminescence. LN229- and GBM#P3-sh-*SChLAP1*-1 or -2 were slower growing than control tumors (Fig. 2D and E), and survival time of tumor-bearing mice was prolonged (LN229: 47 days or 49 days vs. 34 days, sh-*SChLAP1*-1 or sh- *SChLAP1*-2 vs. NC, respectively, $P < 0.01$; GBM#P3: 35 days or 39 days vs. 27 days, sh-*SChLAP1*-1 or sh-*SChLAP1*-2 vs. NC, respectively, $P < 0.01$; Fig. 2F).

These results indicated that *SChLAP1* functioned as a potential oncogene in GBM.

HNRNPL is a protein partner of *SChLAP1* in GBM cells

To identify potential interacting proteins with *SChLAP1* in GBM cells, we performed a biotin-labeled *SChLAP1*-based pull-down assay in LN229 cells followed by proteomic analysis (Fig. 3A). In these assays targeting biotin-labeled RNA, 15 and 29 proteins were found to be associated with sense and antisense *SChLAP1* transcripts, respectively (confidence $\geq$ 95%, unique peptides $\geq$ 1; Supplementary Fig. S2A; Supplementary Table S6). The number of unique proteins associated with *SChLAP1* sense was only 6, and with *SChLAP1* antisense, 20 (Supplementary Fig. S2A). Among the 6 proteins pulled down by *SChLAP1* sense (ENO1, HNRNPL, MCCC2, HSP90AB1, GRSF1, TTBK1), we eliminated MCCC2 and TTBK1 from further analysis because they have not been reported to play an oncogenic role in any human cancers. As the remaining 4 proteins have been previously recognized as tumor promoting (15–20), we silenced ENO1, HNRNPL, HSP90AB1, and GRSF1 in U118MG and LN229 cells using two specific siRNAs for each protein and evaluated cell growth. Knockdown efficiency of the siRNAs was assessed by Western blot analysis (Supplementary Fig. S2B). Over the course of 72 hours, only knockdown of HNRNPL led to significantly decreased proliferation in these two cell lines (Supplementary Fig. S2C). A Western blot incubated with anti-HNRNPL antibody confirmed the association of *SChLAP1* sense with HNRNPL in the pull-down assays targeting the biotin-labeled RNA (Fig. 3B).

We also used an RIP assay to further demonstrate a physical association between the RNA and the protein in LN229 and U118MG cells. Complexes immunoprecipitated this time with antibody against HNRNPL indeed contained *SChLAP1* sense transcripts. These results confirmed HNRNPL as a protein partner of *SChLAP1* in GBM cells (Fig. 3C). To identify the exon(s) of *SChLAP1* that binds HNRNPL in GBM cells, we performed deletion-mapping assays. Exon 2 (338-433 bp) of *SChLAP1*, rather than exons 1, 3, 4, or 5, was key to the formation of the *SChLAP1*–HNRNPL complex (Fig. 3D).

Using a full-length construct, we performed ectopic expression studies in U118MG and BG7 cells, which exhibited low levels of *SChLAP1* (Fig. 1C; Supplementary Fig. S5D), to investigate its role in GBM cell growth. We also used a *SChLAP1* deletion mutant, *SChLAP1*-Δexon2, and *SChLAP1*-AS, to investigate the significance of the *SChLAP1*–HNRNPL interaction in GBM. Transcript levels from all constructs were upregulated approximately 20- to 35-fold (Supplementary Fig. S3A). *SChLAP1* overexpression enhanced the growth of GBM cells both *in vitro* and *in vivo*, while *SChLAP1*-Δexon2 and *SChLAP1*-AS had no effect (Supplementary Fig. S3B–S3D). Overall survival was also reduced in mice bearing U118MG- and BG7-*SChLAP1*-OE tumors relative to control mice (U118MG: 26 days vs. 35 days, *SChLAP1*-OE vs. NC, $P < 0.05$; BG7: 27 days vs. 44 days, *SChLAP1*-OE vs. NC, $P < 0.05$; Supplementary Fig. S3E). However, overall survival remained unchanged in *SChLAP1*-Δexon2- and *SChLAP1*-AS-OE groups (U118MG: 33 or 33 days vs. 35 days, *SChLAP1*-Δexon2-OE or *SChLAP1*-AS-OE vs. NC, P = n.s.; BG7: 47 or 49 days vs. 44 days, *SChLAP1*-Δexon2-OE or *SChLAP1*-AS-OE vs. NC, P = n.s.; Supplementary Fig. S3E).

We also identified the region of the protein binding the RNA. Full-length HNRNPL (64-kDa) has a Gly-rich N-terminal region followed by 4 RNA recognition motifs (RRM): RRM1 (residues 102-176), RRM2 (193-270), RRM3 (382-478), and RRM4 (495-583). Blatter and colleagues introduced a new definition for both RRM2 and RRM3, (v)RRM2 and (v)RRM3, respectively – because these two domains deviate from the canonical RRM structure [2-helix with a four-stranded antiparallel β-sheet (β4β1β3β2)], and present as a C-terminal fifth β-strand (21). When prepared as truncated forms, all four RRM domains of HNRNPL have been shown to bind RNA, and the structures of the complexes have

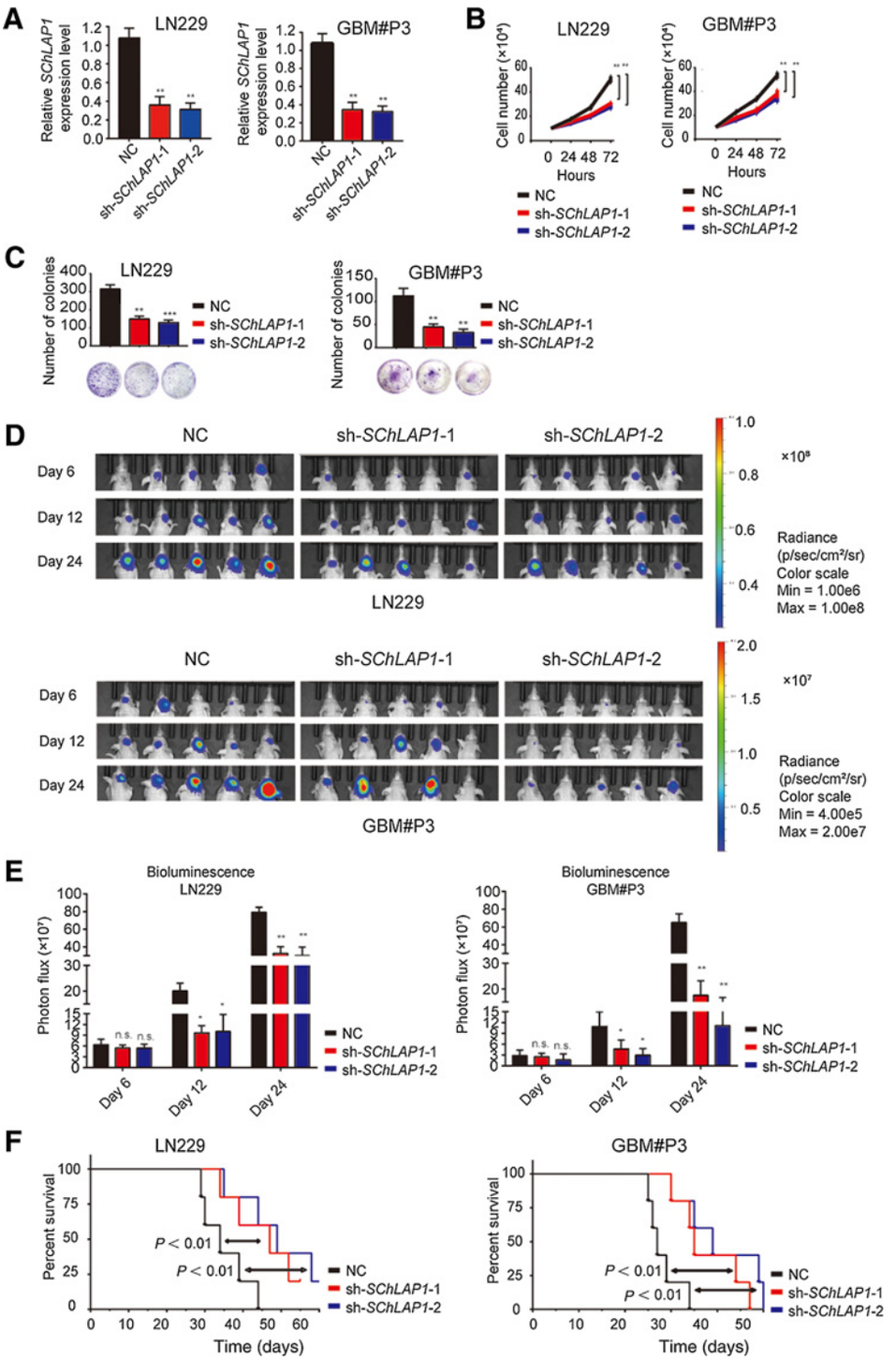

Figure 2.

SChLAP1 promotes the growth of GBM cells *in vitro* and *in vivo*. LN229 and GBM#P3 cells were infected with lentiviral contructs, NC or *SChLAP1* shRNAs. Knockdown efficiency was analyzed with qRT-PCR (**A**). GAPDH served as the internal control. Cell growth was examined in cell counting (**B**) and colony-forming assays (**C**). Data are represented as the mean ± SEM from 3 independent experiments. **D** and **E,** *In vivo* bioluminescent images and quantification of LN229- and GBM#P3-NC and -sh-*SChLAP1*-1 and -2 derived xenografts at the indicated time points. **F,** Kaplan–Meier survival analysis performed with survival data from mice implanted with LN229- and GBM#P3-NC and -sh-*SChLAP1*-1 and -2 cells. Log-rank test, $P < 0.01$. (n.s., not significant; *, $P < 0.05$; **, $P < 0.01$; ***, $P < 0.001$).

been obtained by NMR (21), including the additional β-strand of (v)RRM2 and (v)RRM3 (Supplementary Fig. S4A). The molecular surfaces of the domains, without the bound RNA, can also be predicted on the basis of interpolated charges, showing the positively charged surface areas at the RNA-binding sites (Supplementary Fig. S4A). We therefore prepared 3 truncated forms of HNRNPL: (i) residues 1-189, including RRM1; (ii) residues 1-319, including RRM1 and RRM2; and (iii) 1-489, including RRM2-RRM3. An *in vivo* binding assay indicated that RRM2 of HNRNPL is indispensable for pulling down *SChLAP1* in LN229 and U118MG cells (Fig. 3E).

As an RNA-binding protein (19), HNRNPL has been reported to enhance mRNA stability of genes, such as *VEGF* and *Glut1*, by binding to adenine and uridine-rich elements (ARE) in the

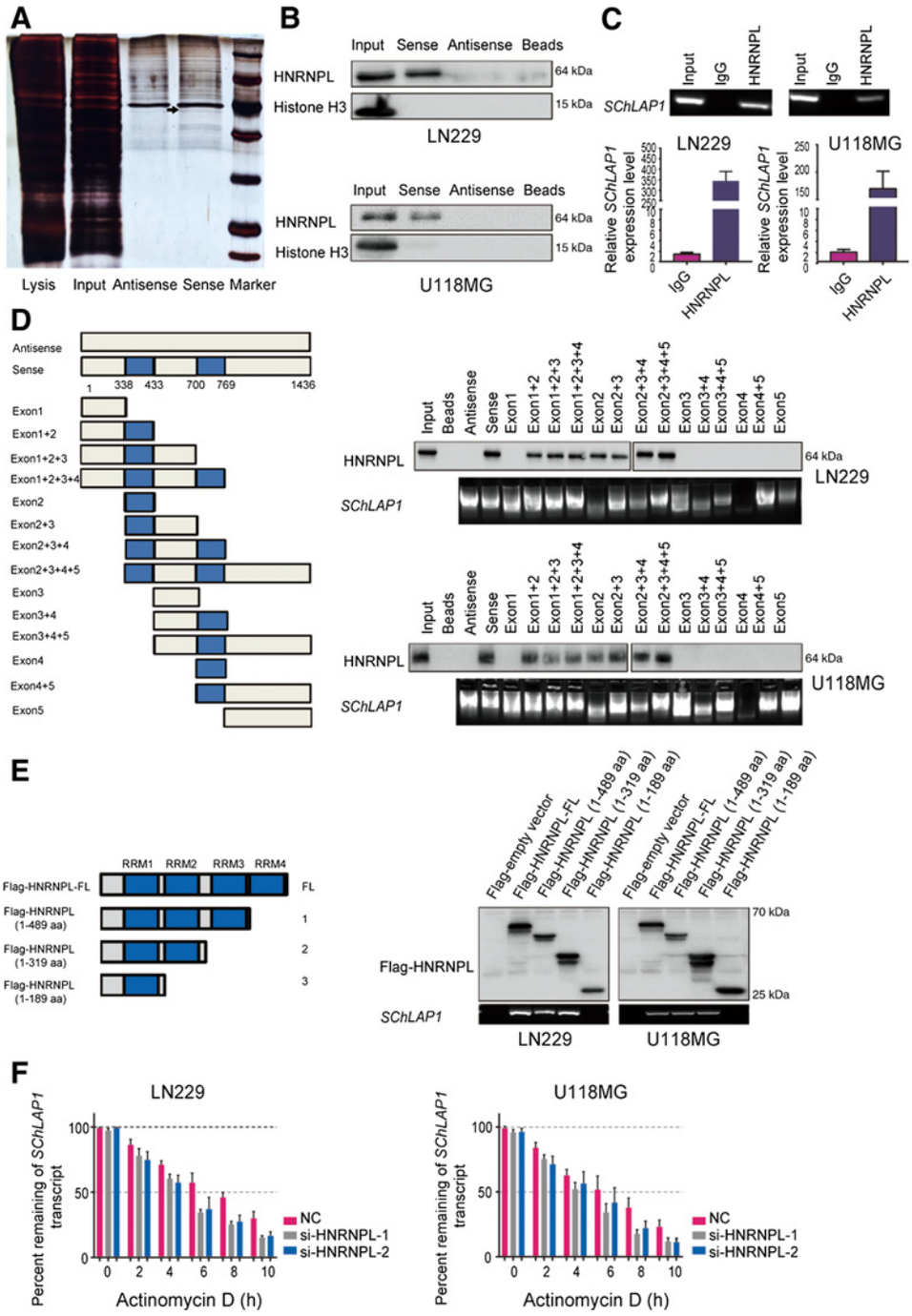

Figure 3.

HNRNPL is a protein partner of *SChLAP1* in GBM cells. **A,** SDS-PAGE resolving proteins from LN229 cell extracts brought down with biotin-labeled *SChLAP1* and antisense RNA. Proteins were excised from gels and submitted for mass spectrometry. **B,** Western blot analysis showing the interaction between *SChLAP1* and HNRNPL. *SChLAP1* antisense and bead-bound protein served as negative controls. **C,** RIP assays performed with LN229 and U118MG cell extracts using anti-HNRNPL or rabbit IgG. IgG served as the negative control. RNAs enriched in anti-HNRNPL or IgG pull-downs were determined relative to input control. **D,** Schematic representation of *SChLAP1* exons used in RNA pull-down assays performed with LN229 and U118MG cell extracts and biotin-labeled *SChLAP1* transcripts. Western blot analysis for HNRNPL pulled down and ethidium stained gel to detect *SChLAP1* transcripts. *SChLAP1* antisense and beads served as negative controls. **E,** Schematic representation of the Flag-tagged HNRNPL domains for RIP assays performed with LN229 and U118MG cell extracts using anti-Flag to examine the interaction between HNRNPL truncates and *SChLAP1.* Flag-empty vector served as the negative control. Western blot analysis for Flag-HNRNPL constructs and ethidium bromide staining for *SChLAP1* RNA on an agarose gel in pull-downs. **F,** Graphic representation of qRT-PCR to determine half-life of *SChLAP1* RNA in cells transfected with HNRNPL or NC siRNAs and incubated with actinomycin D (1 μg/mL) for indicated time.

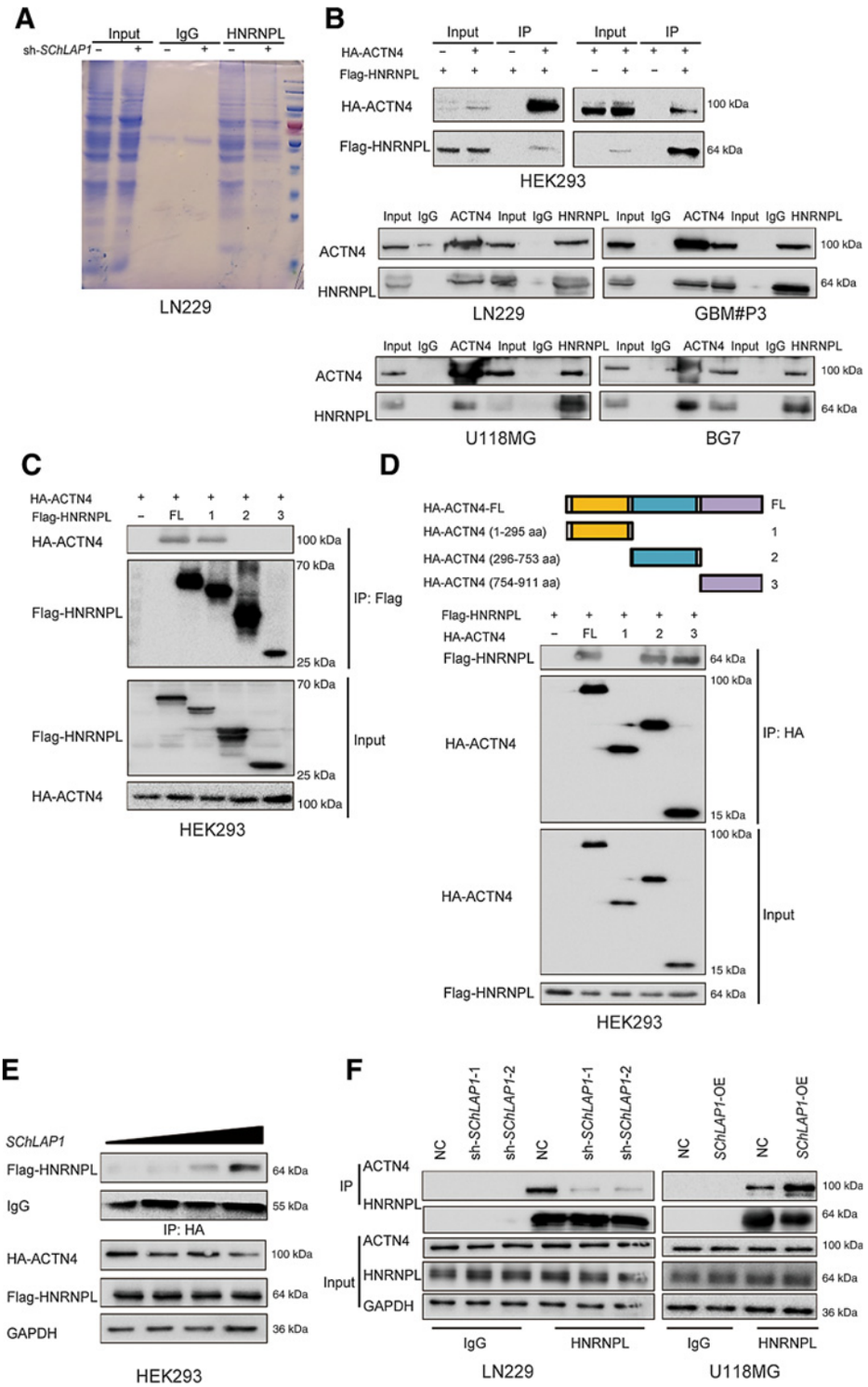

Figure 4.

SChLAP1 regulates the interaction between HNRNPL and ACTN4. **A,** co-IPs performed and analyzed by Commassie blue staining and mass spectrometry identifying ACTN4 as an interacting protein with HNRNPL. **B,** Western blot analysis of co-IPs performed on lysates prepared from HEK293 cells transfected with HA-ACTN4 and Flag-HNRNPL, and parental LN229, U118MG, GBM#P3, and BG7 cells. **C,** Western blot analysis of co-IPs performed on lysates prepared from HEK293 cells transfected with HA-ACTN4 alone or together with indicated Flag-HNRNPL constructs. Top, co-IP performed with anti-Flag; bottom, input protein. **D,** Schematic representation of wild-type ACTN4 and the indicated deletion mutants. Western blot analysis of co-IPs performed on lysates prepared from HEK293 cells transfected with Flag-HNRNPL alone or together with indicated HA-ACTN4 constructs. Top, co-IPs performed with anti-HA; bottom, input protein. **E,** Western blot analysis of co-IPs performed with anti–HA-tag and lysates prepared from HEK293 cells transfected with increasing amounts of *SChLAP1*, and indicated Flag-HNRNPL and HA-ACTN4. Top, corresponds to Western blot for co-IPs; bottom, corresponds to input protein. Cells were pretreated with MG132 (20 μmol/L) for 8 hours. **F,** Western blot analysis of co-IPs performed with anti-HNRNPL and lysates prepared from modified LN229 and U118MG cells. Cells were pretreated with MG132 (20 μmol/L) for 8 hours. IgG groups served as negative controls.

3′UTR, which is a key region for posttranscriptional regulation of RNA stability (22, 23). To examine whether HNRNPL might affect the half-life of *SChLAP1* in GBM cells, we treated LN229-si-*HNRNPL*-1, -2, or -NC cells with actinomycin D (22) and generated an RNA decay curve over the course of 10 hours using qRT-PCR (Fig. 3F). Within 6 hours of addition of actinomycin D, the stability of *SChLAP1* was found to be significantly reduced in LN229-si-*HNRNPL*-1 or -2 cells relative to controls. However, manipulation of *SChLAP1* levels had no effect on HNRNPL protein levels (Supplementary Fig. S4B).

All together, these results demonstrated that HNRNPL stabilized *SChLAP1* through the generation of a protein–RNA complex and might be a critical functional partner of *SChLAP1* in GBM cells. In fact, HNRNPL has been already identified as a partner of the lncRNA THRIL in human disease (24).

SChLAP1 promotes association between HNRNPL and ACTN4

To identify possible protein–protein interactions, which might be regulated by the binding of *SChLAP1* to HNRNPL, we conducted proteomic analysis using lysates prepared from control and *SChLAP1* knockdown cells (LN229-NC and -sh-*SChLAP1*, respectively; Fig. 4A). Mass spectrometry was used to analyze proteins in co-IP complexes brought down with anti-HNRNPL. With confidence $\geq$95% and unique peptides $\geq$1, our analysis produced 764 and 437 putative proteins associated with HNRNPL from LN229-NC and -sh-*SChLAP1* samples, respectively. We selected the top 40 proteins with differential expression between LN229-NC and -sh-*SChLAP1*. Among the 40 proteins chosen, 9 proteins (ACTN4, SPTAN1, PRKDC, ATP5B, SPTBN1, XRCC5, PLEC, hnRNPR, and FSCN1) present in NC samples were significantly reduced in knockdown samples (Supplementary Table S7). Of these, *ACTN4* has been widely recognized as a tumor-promoting gene in a number of human cancers (25–28). In addition, ACTN4 was found to be a protein partner of hnRNPK, a protein that belongs to the same family as HNRNPL, in castration-resistant prostate cancer (29). Furthermore, aberrant expression of lncRNA transcribed from the loci of *ACTN4* has been detected in renal cell carcinoma in a meta-analysis (30). Finally, ACTN4 has been associated with increasing grade and astrocytic differentiation in gliomas based on IHC (31).

Thus, we focused on ACTN4 in the development of human gliomas. IHC performed on our tissue microarray revealed increased ACTN4 to be associated with increased age ($P = 0.0492$), wild-type *IDH1* ($P < 0.001$), positive ATRX staining ($P = 0.0385$), and increasing tumor grade ($P < 0.001$; Supplementary Fig. S5A and S5B; Supplementary Table S8). Greater expression of *ACTN4* was also correlated with poorer overall survival in patients (Supplementary Fig. S5C). Expression of ACTN4 in nonneoplastic brain tissue samples was nearly absent (Supplementary Fig. S5A and S6A).

To demonstrate the physical association between the two proteins, we first performed co-IPs in HEK293 cells with exogenous expression of HA- and Flag-tagged ACTN4 and HNRNPL, respectively. Analysis of the co-IPs on Western blot analysis demonstrated that ACTN4 and HNRNPL physically associated with each other in HEK293 cells (Fig. 4B). Two-way co-IPs performed in LN229, GBM#P3, U118MG, and BG7 cells demonstrated that ACTN4 was a protein partner of HNRNPL in GBM cells, even under conditions of endogenous expression (Fig. 4B).

To identify the regions of the proteins critical for association, we performed co-IPs with HA-ACTN4 and Flag-tagged truncated as well as full-length (FL) HNRNPL, based on the signature protein domains: Flag 1, RRM1-RRM2-RRM3, residues 1-489; Flag 2, RRM1-RRM2, residues 1-319; Flag 3, RRM1, residues 1-189. HA-ACTN4 was only present in co-IPs when the RRM3 domain of HNRNPL was present (Fig. 4C). RRM3 was thus crucial in the formation of the complex between ACTN4 and HNRNPL. We also created HA-tagged ACTN4 domains to test in coIPs with Flag-HNRNPL: HA-ACTN4-1, which has one actin-binding domain, 1-295aa; HA-ACTN4-2, which has a rod domain with four spectrin repeats, 296-753aa; and HA-ACTN4-3, which has a CaM-like domain, 754-911aa. HA-ACTN4-2 and HA-ACTN4-3 pulled down Flag-HNRNPL at a similar efficiency as full-length HA-ACTN4. However, no Flag-HNRNPL was detected when HA-ACTN4-1 was used as input for the co-IP (Fig. 4D). These results indicated that the rod and CaM-like domains were critical elements for complex formation between ACTN4 and HNRNPL.

Finally, we examined the role of *SChLAP1* in formation of the complex between ACTN4 and HNRNPL. Increasing *SChLAP1* led to increased Flag-HNRNPL in pull-downs for HA-ACTN4 in HEK293 cells (Fig. 4E). We also modulated *SChLAP1* with shRNAs (sh-*SChLAP1*-1 and sh-*SChLAP1*-2) in LN229 cells and an expression construct (*SChLAP1*-OE) in U118MG cells, and assessed binding between the two proteins. Knockdown of *SChLAP1* led to reduced binding of HNRNPL to ACTN4 in LN229 cells, while overexpression promoted association between the 2 proteins in U118MG cells (Fig. 4F).

Taken together, these results demonstrated that the lncRNA *SChLAP1* promoted interaction between HNRNPL and ACTN4.

The *SChLAP1*–HNRNPL complex inhibits ubiquitination and proteasomal degradation of ACTN4

To investigate potential functions of this complex, we examined expression of ACTN4 at the RNA and protein levels in response to changes in *SChLAP1*. Changes in *ACTN4* mRNA levels were insignificant regardless of the expression levels of *SChLAP1* in LN229, GBM#P3, U118MG, and BG7 cells (Fig. 5A). However, on Western blot, levels of ACTN4 changed significantly in response to loss or gain of *SChLAP1* (Supplementary Fig. S4B). Furthermore, expression correlation analysis conducted in GBM cell lines and tissue microarrays demonstrated that levels in *SChLAP1* and ACTN4 protein were coordinately regulated (Supplementary Fig. S5D and S5E). These results indicated that loss of *SChLAP1* might enhance ACTN4 protein degradation. However, treatment with the proteasomal inhibitor MG132 reversed the effect of *SCHLAP1* knockdown on the degradation of ACTN4 in LN229 and GBM#P3 cells (Fig. 5B). To examine the half-life of ACTN4 in response to *SChLAP1* expression, gene-modified LN229, GBM#P3, U118MG, and BG7 cells were treated with the protein synthesis inhibitor cycloheximide followed by measurement of ACTN4 protein levels on Western blot analysis. The half-life of ACTN4 was reduced by approximately 4 hours in LN229-sh-*SChLAP1* cells and approximately 2 hours in GBM#P3-sh-*SChLAP1* cells compared with controls (Fig. 5C and D). In contrast, overexpression of *SChLAP1* prolonged the half-life of ACTN4 by approximately 4 hours in U118MG and BG7 cells (Fig. 5C and D). Finally, ubiquitination of ACTN4 in control and modified LN229, GBM#P3, U118MG, and BG7 cells was modulated in parallel based on *SChLAP1* expression. Silencing of *SChLAP1* accelerated endogenous ubiquitination of ACTN4 in LN229 and GBM#P3 cells, while overexpression of *SChLAP1* repressed ubiquitination of ACTN4 in U118MG and BG7 cells (Fig. 5E and F).

In summary, the *SChLAP1*–HNRNPL complex stabilized ACTN4 in GBM cells through inhibition of ubiquitination and consequent proteasomal degradation.

SChLAP1 activates NF-κB signaling by regulating p65 subunit nuclear translocation

To elucidate downstream mechanisms in response to stabilization of ACTN4 in GBM cells, we first performed cluster analysis to identify genes coregulated with *ACTN4*, using the RNA

sequencing data in the CGGA (Supplementary Fig. S7A). In this analysis, 1,046 positively and 668 negatively correlated genes of *ACTN4* were identified ($P < 0.05$). Increased expression of *ACTN4* also correlated with increasing tumor grade, classical TCGA subtype, older age, and wild-type *IDH1* status. These results all together implicated *ACTN4* as an oncogene in glioma progression (Supplementary Fig. S7A). Interestingly, ACTN4 has been reported to function as a transcriptional coactivator of the RelA/p65 subunit of NF-κB (32). In addition, expression of *ACTN4* mRNA was induced by NF-κB in human melanoma

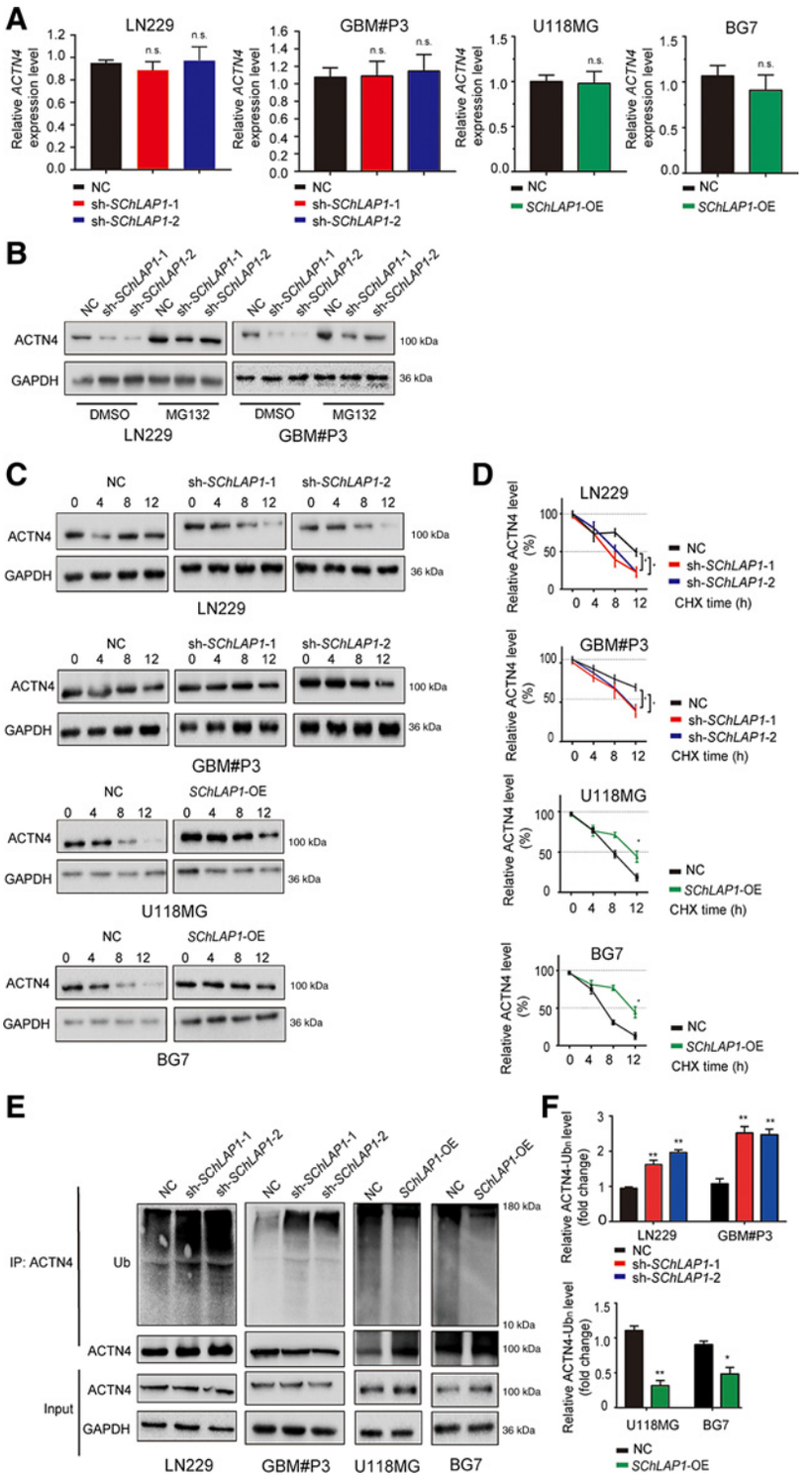

Figure 5.

SChLAP1–HNRNPL complex regulates the proteasomal degradation of ACTN4. **A,** qRT-PCR for *ACTN4* in control and *SChLAP1*-modified LN229, GBM#P3, U118MG, and BG7 cells. **B,** Western blot for ACTN4 in control and *SChLAP1*-modified LN229 and GBM#P3 cells after treatment with MG132 (20 μmol/L). Corresponding dose of DMSO served as the negative control. **C,** Western blot to detect ACTN4 after 0, 4, 8, and 12 hours of cycloheximide (25 μg/mL) treatment in control and *SChLAP1*-modified LN229, GBM#P3, U118MG, and BG7 cells. **D,** Decay curve of ACTN4 protein in control and *SChLAP1*-modified LN229, GBM#P3, U118MG, and BG7 cells based on quantitative analysis of bands in **C** using Image J. **E,** Western blot of ACTN4 IPs using cell lysates isolated from control and *SChLAP1*-modified LN229, GBM#P3, U118MG, and BG7 cells to examine endogenous ACTN4 ubiquitination. **F,** Quantification of ACTN4-Ub_n smear bands in **E** relative to immunoprecipitated ACTN4 protein and NC using Image J (n.s., not significant; *, $P < 0.05$; **, $P < 0.01$).

cells (33). We therefore examined whether there was any overlap between our *ACTN4* correlated genes and the Rel/NF-κB target genes (34) available from a public database (http://bioinfo.lifl.fr/NF-KB/). We found 19 genes to be overlapping between these 2 groups (Supplementary Fig. S7B).

To determine the functional relationship between ACTN4 and NF-κB signaling, we assessed the activity of an NF-κB luciferase reporter construct in response to the *SChLAP1*–HNRNPL–ACTN4 complex in GBM cells. Luciferase activity decreased significantly in LN229-sh-*SChLAP1* cells, but increased in U118MG-*SChLAP1*-OE cells (Supplementary Fig. S7C and S7D). We subsequently examined levels of the p65 subunit of NF-κB in cytoplasmic and nuclear extracts prepared from LN229-sh-*SChLAP1*/-NC and U118MG-*SChLAP1*-OE/-NC cells on Western blot analysis. In LN229-sh-*SChLAP1* cells, almost no differences were detectable for p65 in the cytoplasm relative to controls; however, a significant decrease of p65 was observed in nuclei (Supplementary Fig. S7E). In U118MG-*SChLAP1*-OE cells, nuclear translocation of p65 were increased (Supplementary Fig. S7E). Immunofluorescence with anti-p65 confirmed the positive correlation between expression of *SChLAP1* and nuclear translocation of NF-κB (Supplementary Fig. S7F).

In conclusion, the *SChLAP1*–HNRNPL complex promoted transcriptional activity and nuclear translocation of NF-κB via enhancing ACTN4 stability in GBM cells.

SChLAP1 promotes the growth of GBM through HNRNPL

To examine the dependence of *SChLAP1* function on HNRNPL, we performed rescue studies in U118MG and BG7 cells using HNRNPL knockdown. ACTN4 protein levels were increased in U118MG- and BG7-*SChLAP1*-OE cells, but this effect was abolished in the presence of HNRNPL shRNAs (Fig. 6A). Silencing of HNRNPL also reduced the enhanced proliferation of U118MG- and BG7-*SChLAP1*-OE cells and the elevated transcriptional activity of NF-κB to control levels (Fig. 6B and C).

Finally, we examined whether HNRNPL influenced growth in an intracranial tumor model derived from U118MG- and BG7-*SChLAP1*-OE cells. Growth of U118MG- and BG7-*SChLAP1*-OE tumors was enhanced compared with control tumors, but this effect was abolished by HNRNPL knockdown (Fig. 6D and E). Overall survival was also correspondingly reduced in mice bearing U118MG- and BG7-*SChLAP1*-OE tumors relative to control mice (U118MG: 27 days vs. 39 days, *SChLAP1*-OE vs. NC, $P < 0.05$; BG7: 29 days vs. 44 days, *SChLAP1*-OE vs. NC, $P < 0.05$; Fig. 6F). However, HNRNPL knockdown in the context of *SChLAP1* overexpression brought overall survival back to nearly control levels (U118MG: 44 or 44 days vs. 39 days, *SChLAP1*-OE-sh-HNRNPL-1 or -sh-HNRNPL-2 vs. NC, P = n.s.; BG7: 49 or 39 days vs. 44 days, *SChLAP1*-OE-sh-HNRNPL-1 or -sh-HNRNPL-2 vs. NC, P = n.s.; Fig. 6F).

These results indicated that HNRNPL is a key effector in *SChLAP1*-promoted proliferation of GBM cells *in vitro* and *in vivo*.

Discussion

The detailed molecular analysis of human GBM has revealed a broad spectrum of molecules involved in tumorigenesis with potential for targeted therapy. Here, we found overexpression of an lncRNA, *SChLAP1*, in GBM and demonstrated that loss of *SChLAP1* reduced tumor cell growth *in vitro* and *in vivo* (Fig. 6G). The elevated expression of *SChLAP1* facilitated the formation of a protein complex between HNRNPL with the protein ACTN4 in GBM cells. This complex enhanced stabilization of ACTN4 leading to nuclear accumulation of the p65 subunit of NF-κB and activation of the NF-κB pathway, which is known to be tumor promoting. Points of physical association between the lncRNA and these proteins will enable the future design of small molecules that may be specific for the treatment of human GBM.

The abnormal expression and fundamental functions of the lncRNA family in GBM genesis has implications for their potential as therapeutic targets. For instance, Notch-activated *TUG1* has been shown to promote self-renewal of glioma stem cells (GSCs) by sponging *mir-145* and recruiting polycomb proteins, which results in the repression of genes critical for differentiation (35). Antisense oligonucleotides targeting *TUG1* injected intravenously with the help of a special drug delivery tool successfully suppressed the stemness and growth of GSCs (35). BET proteins have been well-established as viable therapeutic targets in GBM; however, the mechanisms underlying BET inhibitor–regulated GBM progression remain unclear (36). An encouraging study has however demonstrated that the GBM-promoting lncRNA *HOTAIR* can be repressed by treatment with the BET bromdomain inhibitor I-BET151 (36), which further supports the consideration of lncRNAs as novel targets to beat GBM.

HNRNPL has been found to bind lncRNAs, forming a functional complex active in biological processes of human cells. TNFα and HNRNPL related immunoregulatory LincRNA (*THRIL*; also known as Linc1992) was found to bind to HNRNPL, generating a complex that regulates the expression of TNFα at transcriptional and posttranscriptional levels and ultimately mediating response of the innate immune system (24). In another study conducted in hepatocellular carcinoma cells, a complex formed between Lnc*CASC9* (cancer susceptibility 9) and HNRNPL was demonstrated to activate AKT signaling and participate in multiple biological processes, including cell proliferation, apoptosis, and DNA damage (19). These studies concluded that HNRNPL could serve as a protein partner of lncRNAs in human disease. This evidence is consistent with our findings that HNRNPL is a protein partner of *SChLAP1* in GBM cells. Furthermore, HNRNPL stabilized *SChLAP1* when binding to the 338-433nt region (exon 2) through RRM2 (at amino acids 189-319). In fact, HNRNPL was observed to form a 69-kDa protein–RNA complex with the hypoxia stability region of *VEGF*, which is a critical gene promoting angiogenesis in GBM (23). HNRNPL has also been reported to affect the stability of *Glut1* in brain tumor cells. Consistent with these results, we found that HNRNPL also stabilized *SChLAP1* and confirmed a specific interaction between exon 2 of *SChLAP1* and RRM2 of HNRNPL, thus supporting HNRNPL as a protein partner of lncRNA in human cancer cells.

The selectivity for RRM2 may be related to a higher binding affinity of RNA for the fifth β-strand–modified vRRMs providing an extension of the RNA-binding interface, and thus allowing the accommodation of two more nucleotides (37). Therein lies a potential viable therapeutic strategy: to screen for small molecules with satisfying affinity and specificity for the motif of *SChLAP1*, which would potentially inhibit complex formation with HNRNPL. The therapeutic strategy of small molecules targeting RNA binding unfortunately has many significant challenges. However, some critical achievements have already

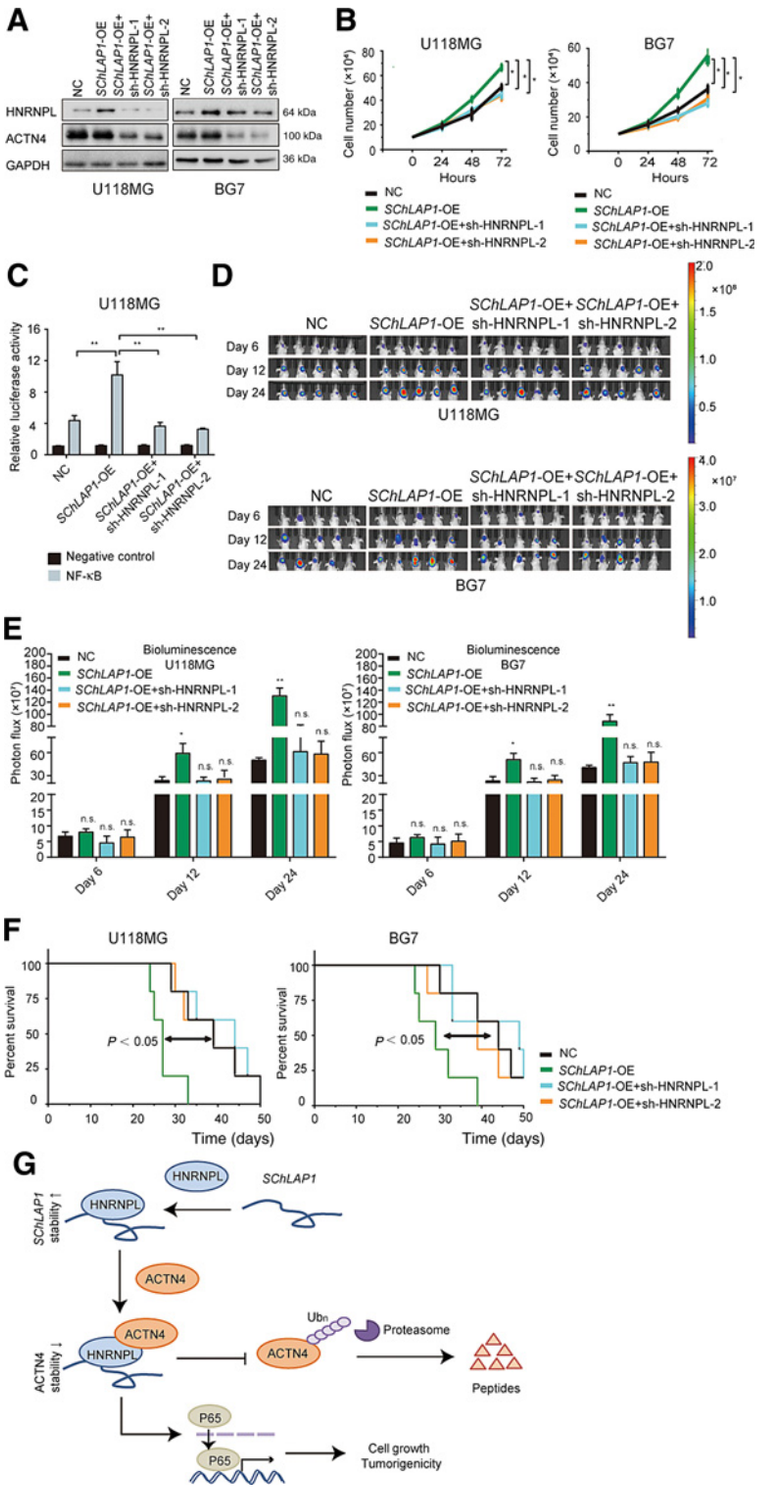

Figure 6.

SChLAP1 promotes the growth of GBM via HNRNPL. **A–C,** Western blot (**A**) to detect HNRNPL and ACTN4 in U118MG- and BG7-*SChLAP1*-OE infected with sh-HNRNPL-1 and sh-HNRNPL-2. U118MG- and BG7-NC, -*SChLAP1*-OE+sh-HNRNPL-1, and -*SChLAP1*-OE+sh-HNRNPL-2 cells in cell growth assay as measured by cell counting (**B**) and luciferase activity from transfected NF-κB luciferase reporter contructs (**C**). **D** and **E,** *In vivo* bioluminescent images and quantification of U118MG- and BG7-NC, -*SChLAP1*-OE+sh-HNRNPL-1 and -2 derived xenografts at the indicated time points. **F,** Kaplan–Meier survival analysis performed with survival data from mice implanted with U118MG- and BG7-NC, -*SChLAP1*-OE+sh-HNRNPL-1 and -2 cells. Log-rank test, *SChLAP1*-OE versus NC: $P < 0.05$; *SChLAP1*-OE+sh-HNRNPL-1 or -2 versus NC: $P =$ n.s. **G,** A graphical model for *SChLAP1*-induced GBM growth. HNRNPL is a protein partner of *SChLAP1*, which enhances its stability. *SChLAP1* promotes binding between HNRNPL and ACTN4, which suppresses proteosomal-mediated degradation of ACTN4. The accumulation of ACTN4 in GBM cells facilitates nuclear translocation of p65, resulting in transcription of NF-κB target genes to drive GBM growth (n.s., not significant; *, $P < 0.05$; **, $P < 0.01$).

been reached in this field, such as the approved linezolid antibiotics, which bind RNA (38), and LMI070, which binds the pre-mRNA for survival of motor neuron 2 (SMN2) to enhance the expression of the protein in patients with spinal muscular atrophy (39, 40).

The key finding to identifying a function for *SChLAP1* in tumor development is the physical association between *SChLAP1*–HNRNPL and the protein ACTN4, which becomes stabilized in this complex through suppression of its proteasomal mediated degradation. Although we identified ACTN4 as a *SChLAP1*-

HNRNPL binding partner using mass spectrometry, many other results support ACTN4 as a putative oncogene in GBM. First, ACTN4 has been previously associated with the development of human cancer. ACTN4 was found to be associated with the protein hnRNPK, another member in the HNRNPL family, in prostate cancer cell lines (29). Second, IHC and *in silico* analysis demonstrated that increased *ACTN4* was associated with more aggressive gliomas and also poorer overall survival in patients. Third, efficient binding between HNRNPL and ACTN4 is promoted by *SChLAP1*, which is also present at signficantly higher levels in GBM.

Finally, the elevated ACTN4 protein appears to induce activation of NF-κB signaling. NF-κB signaling functions as a key driving force underlying many tumor behaviors, such as uncontrolled proliferation, migration and invasion, and resistance to standard therapies (41–44). Furthermore, the activation of NF-κB signaling facilitates transdifferentiation into the mesenchymal molecular GBM subtype, which is highly invasive and radioresistant relative to other molecular subtypes, such as *IDH1/2*-mutated GBM (41). NF-κB signaling has critical cross-talk with the other cancer-related pathways, such as Notch, which is an essential factor in the maintainence of GSC stemness (43). In our study, we found enhanced nuclear translocation of p65 in GBM cells, which leads to activation of NF-κB signaling, to be a downstream event of increased *SChLAP1* expression. These results raise the possibility of targeting the physical association between the proteins HNRNPL and ACTN4 to eliminate the GBM-promoting effects of *SChLAP1*. In addition, we have identified the specific structural HNRNPL and ACTN4 domains that mediate their interaction. Thus, our work may have more practical implications for clinical use, as small molecules are more easily developed to effectively target protein complexes compared with RNAs.

In summary, we identified *SChLAP1* as a growth-promoting lncRNA in GBM and as a potential therapeutic target in GBM treatment. Our study thus establishes a basis for pursuing the development of lncRNA-oriented cancer therapies, especially for treatment of GBM.

Disclosure of Potential Conflicts of Interest

No potential conflicts of interest were disclosed.

Authors' Contributions

Conception and design: J. Ji, R. Xu, A. Chen, X. Li, J. Wang
Development of methodology: J. Ji, R. Xu, G. Bao, Xiuying Wang
Acquisition of data (provided animals, acquired and managed patients, provided facilities, etc.): J. Ji, B. Huang, Xinyu Wang, A. Chen
Analysis and interpretation of data (e.g., statistical analysis, biostatistics, computational analysis): J. Ji, K. Ding, G. Bao, X. Zhang, A. Martinez, Xiuying Wang, H. Miletic
Writing, review, and/or revision of the manuscript: J. Ji, R. Xu, G. Bao, Xiuying Wang, F. Thorsen, R. Bjerkvig, J. Wang
Administrative, technical, or material support (i.e., reporting or organizing data, constructing databases): J. Ji, G. Li, F. Thorsen, R. Bjerkvig, L. Xiang, B. Han
Study supervision: A. Chen, X. Li, J. Wang

Acknowledgments

This work was supported by the National Natural Science Foundation of China (81702474), the Department of Science & Technology of Shandong Province (2017CXGC1502, 2017CXGC1504, 2016GSF201060, and 2018GSF118082), the Special Foundation for Taishan Scholars (ts20110814 and tshw201502056), the Shandong Provincial Natural Science Foundation (ZR2017MH116), the China Postdoctoral Science Foundation (2018M642666), the Jinan Science and Technology Bureau of Shandong Province (201704096), the University of Bergen, the Nowegian Cancer Society, and the K.G. Jebsen Brain Tumor Research Center.

The costs of publication of this article were defrayed in part by the payment of page charges. This article must therefore be hereby marked *advertisement* in accordance with 18 U.S.C. Section 1734 solely to indicate this fact.

Received March 4, 2019; revised June 25, 2019; accepted August 15, 2019; published first September 6, 2019.

References

1. Lapointe S, Perry A, Butowski NA. Primary brain tumours in adults. Lancet 2018;392:432–46.
2. Sulman EP, Ismaila N, Armstrong TS, Tsien C, Batchelor TT, Cloughesy T, et al. Radiation therapy for glioblastoma: american society of clinical oncology clinical practice guideline endorsement of the american society for radiation oncology guideline. J Clin Oncol 2017;35:361–9.
3. Stupp R, Hegi ME, Mason WP, van den Bent MJ, Taphoorn MJ, Janzer RC, et al. Effects of radiotherapy with concomitant and adjuvant temozolomide versus radiotherapy alone on survival in glioblastoma in a randomised phase III study: 5-year analysis of the EORTC-NCIC trial. Lancet Oncol 2009;10:459–66.
4. Ozdemir-Kaynak E, Qutub AA, Yesil-Celiktas O. Advances in glioblastoma multiforme treatment: new models for nanoparticle therapy. Front Physiol 2018;9:170.
5. Witsch E, Sela M, Yarden Y. Roles for growth factors in cancer progression. Physiology 2010;25:85–101.
6. Wang KC, Chang HY. Molecular mechanisms of long noncoding RNAs. Mol Cell 2011;43:904–14.
7. Peng Z, Liu C, Wu M. New insights into long noncoding RNAs and their roles in glioma. Mol Cancer 2018;17:61.
8. Chen Q, Cai J, Wang Q, Wang Y, Liu M, Yang J, et al. Long noncoding RNA NEAT1, regulated by the EGFR pathway, contributes to glioblastoma progression through the WNT/beta-catenin pathway by scaffolding EZH2. Clin Cancer Res 2018;24:684–95.
9. Zhang R, Jin H, Lou F. The long non-coding RNA TP73-AS1 interacted with miR-142 to modulate brain glioma growth through HMGB1/RAGE pathway. J Cell Biochem 2018;119:3007–16.
10. Saladi SV, Ross K, Karaayvaz M, Tata PR, Mou H, Rajagopal J, et al. ACTL6A Is co-amplified with p63 in squamous cell carcinoma to drive YAP activation, regenerative proliferation, and poor prognosis. Cancer Cell 2017;31:35–49.
11. Reisman D, Glaros S, Thompson EA. The SWI/SNF complex and cancer. Oncogene 2009;28:1653–68.
12. Kadoch C, Crabtree GR. Reversible disruption of mSWI/SNF (BAF) complexes by the SS18-SSX oncogenic fusion in synovial sarcoma. Cell 2013; 153:71–85.
13. Ji J, Xu R, Zhang X, Han M, Xu Y, Wei Y, et al. Actin like-6A promotes glioma progression through stabilization of transcriptional regulators YAP/TAZ. Cell Death Dis 2018;9:517.
14. Yang J, Yan R, Roy A, Xu D, Poisson J, Zhang Y. The I-TASSER Suite: protein structure and function prediction. Nat Methods 2015; 12:7–8.
15. Chen S, Zhang Y, Wang H, Zeng YY, Li Z, Li ML, et al. WW domain-binding protein 2 acts as an oncogene by modulating the activity of the glycolytic enzyme ENO1 in glioma. Cell Death Dis 2018;9:347.
16. Coskunpinar E, Akkaya N, Yildiz P, Oltulu YM, Aynaci E, Isbir T, et al. The significance of HSP90AA1, HSP90AB1 and HSP90B1 gene polymorphisms in a Turkish population with non-small cell lung cancer. Anticancer Res 2014;34:753–7.

17. de la Mare JA, Jurgens T, Edkins AL. Extracellular Hsp90 and TGFbeta regulate adhesion, migration and anchorage independent growth in a paired colon cancer cell line model. BMC Cancer 2017;17:202.
18. Guo J, Lv J, Liu M, Tang H. miR-346 Up-regulates argonaute 2 (AGO2) protein expression to augment the activity of other MicroRNAs (miRNAs) and contributes to cervical cancer cell malignancy. J Biol Chem 2015;290: 30342–50.
19. Klingenberg M, Gross M, Goyal A, Polycarpou-Schwarz M, Miersch T, Ernst AS, et al. The long noncoding RNA cancer susceptibility 9 and RNA binding protein heterogeneous nuclear ribonucleoprotein L form a complex and coregulate genes linked to AKT signaling. Hepatology 2018;68:1817–32.
20. Zhan P, Wang Y, Zhao S, Liu C, Wang Y, Wen M, et al. FBXW7 negatively regulates ENO1 expression and function in colorectal cancer. Lab Invest 2015;95:995–1004.
21. Blatter M, Dunin-Horkawicz S, Grishina I, Maris C, Thore S, Maier T, et al. The signature of the five-stranded vRRM fold defined by functional, structural and computational analysis of the hnRNP L protein. J Mol Biol 2015;427:3001–22.
22. Hamilton BJ, Nichols RC, Tsukamoto H, Boado RJ, Pardridge WM, Rigby WF. hnRNP A2 and hnRNP L bind the 3′UTR of glucose transporter 1 mRNA and exist as a complex in vivo. Biochem Biophys Res Commun 1999;261:646–51.
23. Shih SC, Claffey KP.Regulation of human vascular endothelial growth factor mRNA stability in hypoxia by heterogeneous nuclear ribonucleoprotein L. J Biol Chem 1999;274:1359–65.
24. Li Z, Chao TC, Chang KY, Lin N, Patil VS, Shimizu C, et al. The long noncoding RNA THRIL regulates TNFalpha expression through its interaction with hnRNPL. Proc Natl Acad Sci U S A 2014;111:1002–7.
25. Gao Y, Li G, Sun L, He Y, Li X, Sun Z, et al. ACTN4 and the pathways associated with cell motility and adhesion contribute to the process of lung cancer metastasis to the brain. BMC Cancer 2015;15:277.
26. Liao Q, Li R, Zhou R, Pan Z, Xu L, Ding Y, et al. LIM kinase 1 interacts with myosin-9 and alpha-actinin-4 and promotes colorectal cancer progression. Br J Cancer 2017;117:563–71.
27. Liu X, Chu KM. alpha-Actinin-4 promotes metastasis in gastric cancer. Lab Invest 2017;97:1084–94.
28. Wang N, Wang Q, Tang H, Zhang F, Zheng Y, Wang S, et al. Direct inhibition of ACTN4 by ellagic acid limits breast cancer metastasis via regulation of beta-catenin stabilization in cancer stem cells. J Exp Clin Cancer Res 2017;36:172.
29. Capaia M, Granata I, Guarracino M, Petretto A, Inglese E, Cattrini C, et al. A hnRNP K(-)AR-related signature reflects progression toward castration-resistant prostate cancer. Int J Mol Sci 2018;19:pii:E1920.
30. Fachel AA, Tahira AC, Vilella-Arias SA, Maracaja-Coutinho V, Gimba ER, Vignal GM, et al. Expression analysis and in silico characterization of intronic long noncoding RNAs in renal cell carcinoma: emerging functional associations. Mol Cancer 2013;12:140.
31. Fukushima S, Yoshida A, Honda K, Maeshima AM, Narita Y, Yamada T, et al. Immunohistochemical actinin-4 expression in infiltrating gliomas: association with WHO grade and differentiation. Brain Tumor Pathol 2014;31:11–6.
32. Aksenova V, Turoverova L, Khotin M, Magnusson KE, Tulchinsky E, Melino G, et al. Actin-binding protein alpha-actinin 4 (ACTN4) is a transcriptional co-activator of RelA/p65 sub-unit of NF-kB. Oncotarget 2013;4:362–72.
33. Zhang YY, Tabataba H, Liu XY, Wang JY, Yan XG, Farrelly M, et al. ACTN4 regulates the stability of RIPK1 in melanoma. Oncogene 2018;37: 4033–45.
34. Pahl HL. Activators and target genes of Rel/NF-kappaB transcription factors. Oncogene 1999;18:6853–66.
35. Katsushima K, Natsume A, Ohka F, Shinjo K, Hatanaka A, Ichimura N, et al. Targeting the Notch-regulated non-coding RNA TUG1 for glioma treatment. Nat Commun 2016;7:13616.
36. Pastori C, Kapranov P, Penas C, Peschansky V, Volmar CH, Sarkaria JN, et al. The Bromodomain protein BRD4 controls HOTAIR, a long noncoding RNA essential for glioblastoma proliferation. Proc Natl Acad Sci U S A 2015;112:8326–31.
37. Oberstrass FC, Auweter SD, Erat M, Hargous Y, Henning A, Wenter P, et al. Structure of PTB bound to RNA: specific binding and implications for splicing regulation. Science 2005;309:2054–7.
38. Warner KD, Hajdin CE, Weeks KM. Principles for targeting RNA with drug-like small molecules. Nat Rev Drug Discov 2018;17:547–58.
39. Mullard A. Small molecules against RNA targets attract big backers. Nat Rev Drug Discov 2017;16:813–5.
40. Sivaramakrishnan M, McCarthy KD, Campagne S, Huber S, Meier S, Augustin A, et al. Binding to SMN2 pre-mRNA-protein complex elicits specificity for small molecule splicing modifiers. Nat Commun 2017;8: 1476.
41. Bhat KPL, Balasubramaniyan V, Vaillant B, Ezhilarasan R, Hummelink K, Hollingsworth F, et al. Mesenchymal differentiation mediated by NF-kappaB promotes radiation resistance in glioblastoma. Cancer Cell 2013;24:331–46.
42. Hai L, Zhang C, Li T, Zhou X, Liu B, Li S, et al. Notch1 is a prognostic factor that is distinctly activated in the classical and proneural subtype of glioblastoma and that promotes glioma cell survival via the NF-kappaB (p65) pathway. Cell Death Dis 2018;9:158.
43. Kesanakurti D, Chetty C, Rajasekhar Maddirela D, Gujrati M, Rao JS. Essential role of cooperative NF-kappaB and Stat3 recruitment to ICAM-1 intronic consensus elements in the regulation of radiation-induced invasion and migration in glioma. Oncogene 2013;32: 5144–55.
44. Kim SH, Ezhilarasan R, Phillips E, Gallego-Perez D, Sparks A, Taylor D, et al. Serine/threonine kinase MLK4 determines mesenchymal identity in glioma stem cells in an NF-kappaB-dependent manner. Cancer Cell 2016; 29:201–13.